Acta Oceanol. Sin., 2019, Vol. 38, No. 4, P. 146–153
https://doi.org/10.1007/s13131-019-1394-6
http://www.hyxb.org.cn
E-mail: hyxbe@263.net

The Island Rule with lateral and bottom friction

Yanzhao Yang[1, 2], Zexun Wei[1, 3, 4]*, Guanlin Wang[1, 3, 4], Zhan Lian[3, 4], Liwei Wang[1]

[1] College of Meteorology and Oceanography, National University of Defense Technology, Nanjing 211101, China

[2] College of Mathematical Science and Physics, Qingdao University of Science and Technology, Qingdao 266061, China

[3] Key Laboratory of Marine Science and Numerical Modeling, First Institute of Oceanography, Ministry of Natural Resources, Qingdao 266061, China

[4] Laboratory for Regional Oceanography and Numerical Modeling, Pilot National Laboratory for Marine Science and Technology (Qingdao), Qingdao 266237, China

Received 6 June 2018; accepted 25 August 2018

Abstract

The Island Rule, derived from the Sverdrup theory, is widely used to estimate and analyze water transport through a strait. Previous studies presented single- or multi-island rules with either lateral or bottom friction. In this paper, an analytical model of wind-driven circulation is assumed based on linear dynamics. Considering both lateral and bottom friction, the analytic solutions of the transport streamfunction around the islands are derived and the volume transport through the channel is presented. The results are similar to those of Wajsowicz, but the frictional constants represent different values. The analytic solution shows that the relationship between the lateral frictional and bottom frictional dissipation is complex in terms of the frictional constants. To understand the interaction between the two friction types, lateral and bottom friction values were randomly chosen on a barotropic beta plane. The result shows an approximately linear relationship between the lateral and bottom friction in consisting of the combined frictional constants. We studied the effect of the channel width on the transport through the channel. The results show that the friction enhances the flow under some widths, which is similar to the flow behavior when only the lateral friction is considered. We also compared the transport through the channel at different depths and founded that the deeper the water, the smaller the transport reduction ratio when the horizontal eddy viscosity coefficient and the bottom drag coefficient remained constants. To further present the combined role of lateral frictional and bottom frictional dissipation, we compared our model with the model of Wajsowicz for two islands, where only the lateral or bottom friction were considered, with different channel widths. The results showed that the effect of the lateral friction is greater than the bottom friction when the channel is narrow, especially in the Munk boundary layer thickness. When the channel is much wider than the Munk boundary layer thickness, the role of the bottom friction is greater than that of the lateral friction. The model was applied to the Indonesian throughflow and yielded a reduction of approximately 20% in the transport.

Key words: Island Rule, lateral friction, bottom friction, transport streamfunction

Citation: Yang Yanzhao, Wei Zexun, Wang Guanlin, Lian Zhan, Wang Liwei. 2019. The Island Rule with lateral and bottom friction. Acta Oceanologica Sinica, 38(4): 146–153, doi: 10.1007/s13131-019-1394-6

1 Introduction

The Island Rule was derived by Godfrey (1989), who proposed an indirect estimation of the wind-driven transport between an island and an eastern basin boundary, based on the Sverdrup model with linear western boundary dynamics. One of the most successful applications of the rule was in the calculation of the Indonesian throughflow (ITF) transport, which estimated the transport as (16±4)×10^6 m^3/s (Godfrey, 1989; Wajsowicz, 1993). This estimation agrees with later calculations of geostrophic transport (Wijffels et al., 1996) and depth-integrated transport from direct measurement of current (Gordon et al., 1999, 2010).

The limitation of Godfrey's Island Rule is that it assumes that all western ocean boundaries are remote; therefore, it cannot be applied to islands located within the western boundary layer, where the friction along the coast of the island should be taken into account. This issue was studied by Wajsowicz (1993), who considered the lateral or bottom friction based on the Munk-Stommel model. The effects of friction within a narrow passage were discussed by Pedlosky et al. (1997) and Pratt and Pedlosky (1998), showing a similar solution to that of Godfrey's model but with less transport through a narrow strait.

The Island Rule was extended to consider the bottom topography (Wajsowicz, 1993; Lian et al., 2017), multi-islands (Wajsowicz, 2002) and time-dependency (Wajsowicz, 2010; Firing et al., 1999; Pedlosky and Spall, 1997), greatly extending the

Foundation item: The National Key Research and Development Program of China under contract No. 2016YFC0301103; the Scientific and Technological Innovation Project financially supported by Qingdao National Laboratory for Marine Science and Technology under contract No. 2015ASKJ01; the SOA Program on Global Change and Air-Sea Interactions under contract Nos GASI-IPOVAI-03, GASI-IPOVAI-02 and GASI-IPOVAI-01-02; the National Natural Science Foundation of China under contract Nos 40476025, 41876027 and 41506036; the Office of Naval Research of United States under contract No. N00014-08-01-0618.
*Corresponding author, E-mail: weizx@fio.org.cn

applicability of the theory. Wajsowicz (1993, 2002) studied the role of the bottom topography through numerical experiments and theoretical research and analyzed the changes in sea transport volume with variable topography. Studying Atlantic and Caribbean circulation, she expanded the Island Rule to form the Multi-island Rule which includes the effect of bottom friction. By adding the time evolution, Firing et al. (1999) modeled the basic trend of water transport volume in the coastal area of Hawaii. Yang et al. (2013) extended the steady-state island rule to include seasonal variations and applied the new model to explain the relationship between the Luzon Strain transport and the North Equatorial Current bifurcation latitude. The model of Pedlosky and Spall (1997) included the influence of different island shapes on the transport volume.

The Island Rule was tested and applied to different sea areas. For example, Chen et al. (2014) obtained the transport streamfunctions along the eastern coast of Africa. Cai (2006) calculated the distribution of the transport streamfunctions in the Southern Ocean to study the characteristics of the Southern Ocean supergyre circulation. Seung (2003) studied the dynamics of the Tsushima Current by modifying the island theory. Although the island theory has been applied to various types of sea areas, it has been used most widely to analyze the ITF and the surrounding circulation in the West Pacific warm pool (Godfrey, 1989, 1996; Wajsowicz, 1994). The West Pacific warm pool includes many islands and has an important effect on global climate change (Gordon et al., 2003). Different aspects of the island theory have been studied. Qu et al. (Qu, 2000; Qu et al., 2006) explained the upper-layer circulation and the heat and freshwater conveyor in the South China Sea. Qu et al. (2004) studied the role of the Luzon Strait transport in conveying the influence of the El Niño Southern Oscillation to the South China Sea. Liu et al. (2012) explored the link between the local monsoon system and the upper thermal structure in the South China Sea throughflow. By analyzing segments of the integration path of the wind stress, Wang et al. (2006) found the interannual variability of the South China Sea throughflow and Liu et al. (2010) explored the covariation between the South China Sea throughflow and the ITF. Pratt and Pedlosky (1998) studied the Island Rule with lateral friction, focusing on the flow enhancement produced by the lateral friction. Using the same method, they also presented the Island Rule with bottom friction. By comparing the width of the channel with the friction boundary layer thickness, they could model various channels with lateral friction or bottom friction in the real ocean.

In the studies mentioned above where the island theory is applied, friction is omitted (Liu et al., 2012) or only one type of friction is considered (Wajsowicz, 1993, 2002; Pratt and Pedlosky, 1998). In practical applications, there are channels such as the English Channel where both bottom and lateral friction affect the flow (Pratt and Pedlosky, 1998). In such cases it is difficult to choose the type of friction and identify its effect. This paper is based on the studies of Wajsowicz (1993, 2002) on the general ocean circulation. Considering both lateral friction and bottom friction, we derive the extended Island Rule. When the lateral friction coefficient or bottom friction coefficient is zero, the conclusions are similar to the Island Rule of Wajsowicz (1993); thus, our conclusions include and extend the results of Wajsowicz (1993).

The paper is arranged as follows. In Section 2, the basic Island Rule (Godfrey, 1989) is reviewed with several extensions rederived. The analytical results of the transport streamfunction are obtained and the frictional values between two islands are derived by considering the Munk-Stommel model. In Section 3, the factors that form the combined frictional constants are analyzed and the conclusions on the interaction of lateral friction and bottom friction are drawn. In Section 4, to explore the role of bottom and lateral friction dissipation, we compare and discuss the model of Wajsowicz for two islands with different channel widths. In Section 5, our model is applied to the ITF and the reduced transport due to lack of friction is calculated. A discussion and summary are presented in Section 6.

2 The Munk-Stommel model

The model in the study follows Wajsowicz (1993), with two islands lying in the basin, one of the islands partially sheltering the other island (Fig. 1). The ocean is assumed to be stagnant below a certain depth, all the bottom topography is assumed confined and the flow is modeled in terms of quasi-steady motion. The surface wind stress is the only external force. The friction is assumed to be negligible away from the western boundary layer, but has an effect on the flow when the flow passes through the channel between the islands. Let ψ denote the transport streamfunction of the active layer, then the depth-integrated zonal and meridional velocities for the layer are given by $\frac{\partial \psi}{\partial y} = -\int_{-H_0}^{0} u\mathrm{d}z$ and $\frac{\partial \psi}{\partial x} = \int_{-H_0}^{0} v\mathrm{d}z$, where H_0 is a constant, representing the depth of the flat-bottomed ocean. Then, the depth-integrated momentum equations (Pedlosky, 1996) are

$$f\frac{\partial \psi}{\partial x} - \frac{1}{\rho_0}\frac{\partial P}{\partial x} + F^{(x)} + \frac{\tau^{(x)}}{\rho_0} = 0, \tag{1}$$

$$f\frac{\partial \psi}{\partial y} - \frac{1}{\rho_0}\frac{\partial P}{\partial y} + F^{(y)} + \frac{\tau^{(y)}}{\rho_0} = 0, \tag{2}$$

where f is the Coriolis parameter; P is the depth-integrated pressure; ρ_0 is the characteristic density of the ocean; $\vec{F} = \left(F^{(x)}, F^{(y)}\right)$ is the depth-integrated friction term and $\vec{\tau} = \left(\tau^{(x)}, \tau^{(y)}\right)$ is the wind stress. The number of boundary conditions depends on the form of F. Under no-normal flow conditions ψ is a constant at the boundaries.

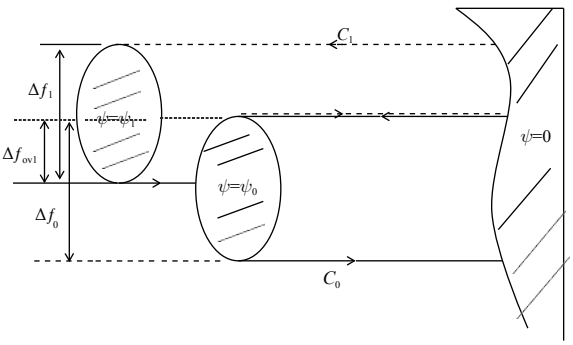

Fig. 1. Sketch of the islands and landmass used in the model. The islands are remote from the western boundary. The paths C_0 and C_1 are the enclosed paths flowing anticlockwise.

The streamfunctions ψ_0 and ψ_1 flow around the islands to the west of the landmass upon which ψ=0, yielding:

$$\psi_0 = \psi_{0,\,\mathrm{ideal}} + \frac{1}{\Delta f_0}\int_A^B \vec{F}\cdot\mathrm{d}\vec{l}, \tag{3}$$

$$\psi_1 = \frac{\Delta f_{\text{ov1}}}{\Delta f_1}\psi_{0,\text{ideal}} + \frac{-1}{\Delta f_1}\oint_{C_1}\frac{\vec{\tau}}{\rho_0}\cdot \mathrm{d}\vec{l} - \left(\frac{\Delta f_0}{\Delta f_1} - \frac{\Delta f_{\text{ov1}}}{\Delta f_1}\right)\frac{1}{\Delta f_0}\int_A^B \vec{F}\cdot \mathrm{d}\vec{l}, \tag{4}$$

where

$$\psi_{0,\text{ideal}} = \frac{-1}{\Delta f_0}\oint_{C_0}\frac{\vec{\tau}}{\rho_0}\cdot \mathrm{d}\vec{l},$$

$$\psi_{1,\text{ideal}} = \frac{\Delta f_{\text{ov1}}}{\Delta f_1}\psi_{0,\text{ideal}} + \frac{-1}{\Delta f_1}\oint_{C_1}\frac{\vec{\tau}}{\rho_0}\cdot \mathrm{d}\vec{l},$$

indicate the ideal streamfunctions when the friction is neglected. Δf_0 and Δf_1 represent the difference between the Coriolis parameter at the northern and southern ends of the northern and southern islands, respectively. Δf_{ov1} is the difference between the Coriolis parameter at the northern and southern ends of the overlapping region of the islands (Fig. 1). C_0 and C_1 are the enclosed pathways.

Equations (3) and (4) show that the streamfunctions depend on the form of the friction. Previous studies considered either the lateral or bottom friction, in terms of $\vec{F} = A_{\text{H}}\nabla^2\vec{v}$ or $\vec{F} = -D_{\text{f}}\vec{v}$, where A_{H} and D_{f} are the horizontal eddy viscosity coefficient and bottom drag coefficient, respectively. They are given as Eqs (4.1)–(4.5) in Wajsowicz (1993). To explore the interaction between the lateral and bottom friction and their influence on ψ, we performed analysis combining both types of friction. The conclusions extend the formulation of Wajsowicz (1993) or Pratt and Pedlosky (1998).

To model the fluid in the basin, we consider the depth-integration Munk-Stommel model:

$$A_{\text{H}}\nabla^4\psi - A_{\text{S}}\nabla^2\psi - \beta\frac{\partial\psi}{\partial x} = -\text{curl}\left(\frac{\vec{\tau}}{\rho_0}\right), \tag{5}$$

where $A_{\text{S}} = \dfrac{D_{\text{f}}}{H_0}$. Following Pratt and Pedlosky (1998) or Wajsowicz (1993), the area between the islands is modeled by a single channel of length L and width W; we assume that $W/L \ll 1$, so that $\dfrac{\partial}{\partial x} \gg \dfrac{\partial}{\partial y}$ in the barotropic equation as shown in Fig. 2. Equation (5) becomes

$$A_{\text{H}}\frac{\partial^4\psi}{\partial^4 x} - A_{\text{S}}\frac{\partial^2\psi}{\partial^2 x} - \beta\frac{\partial\psi}{\partial x} = -\text{curl}\left(\frac{\vec{\tau}}{\rho_0}\right). \tag{6}$$

The wind stress term in Eq. (6) causes a Sverdrup flow which is much smaller than the total transport in the channel (Pratt and Pedlosky, 1998). Therefore, neglecting the right-hand term would not cause a significant error. Using the Cardano formula, the solutions to Eq. (6) have different forms under different conditions.

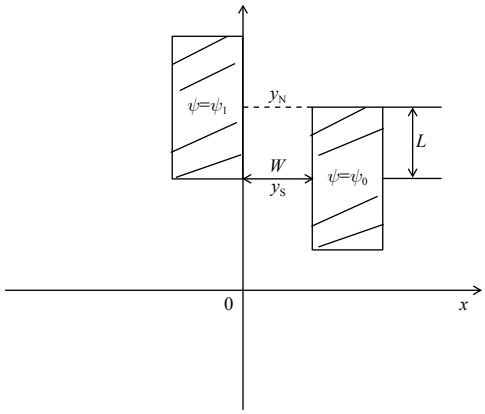

Fig. 2. The coordinate system and the channel between the islands. The single channel is shallow and narrow and the width is much shorter than the length.

When $\left(-\dfrac{\beta}{2A_{\text{H}}}\right)^2 - \left(\dfrac{A_{\text{S}}}{3A_{\text{H}}}\right)^3 < 0$, solving the corresponding homogeneous equation subject to the boundary conditions:

$$\begin{aligned}
&\psi(0,y) = \psi_1,\\
&\left(\frac{\partial\psi}{\partial x}\right)_{x=0} = 0,\\
&\psi(W,y) = \psi_0,\\
&\left(\frac{\partial\psi}{\partial x}\right)_{x=W} = 0.
\end{aligned}$$

We obtain the transport streamfunction between the islands:

$$\psi(x,y) = c_0 + c_1\mathrm{e}^{r_1 x} + c_2\mathrm{e}^{r_2 x} + c_3\mathrm{e}^{r_3 x},$$

where r_1, r_2 and r_3 are the solutions of the characteristic equation:

$$A_{\text{H}}r^3 - A_{\text{S}}r - \beta = 0;$$

c_0, c_1, c_2 and c_3 are determined by the equations:

$$\begin{aligned}
&c_0 + c_1 + c_2 + c_3 = \psi_1,\\
&c_0 + c_1\mathrm{e}^{r_1 W} + c_2\mathrm{e}^{r_2 W} + c_3\mathrm{e}^{r_3 W} = \psi_0,\\
&c_1 r_1 + c_2 r_2 + c_3 r_3 = 0,\\
&c_1 r_1\mathrm{e}^{r_1 W} + c_2 r_2\mathrm{e}^{r_2 W} + c_3 r_3\mathrm{e}^{r_3 W} = 0.
\end{aligned} \tag{7}$$

Then, the dissipation along the integration path can be calculated as

$$\begin{aligned}
F_0 &= \frac{1}{\Delta f_0}\int_A^B \vec{F}\cdot \mathrm{d}\vec{l} \approx \frac{1}{\Delta f_0}\int_A^B \left[A_{\text{H}}\left(\frac{\partial^3\psi}{\partial x^3}\right)_{x=W} - A_{\text{S}}\left(\frac{\partial\psi}{\partial x}\right)_{x=W}\right]\mathrm{d}y\\
&= \frac{(y_{\text{B}} - y_{\text{A}})}{\Delta f_0}\frac{r_1 r_2 r_3}{|A|}\left[\left(A_{\text{H}}r_1^2 - A_{\text{S}}\right)\left(\mathrm{e}^{(r_1+r_3)W} - \mathrm{e}^{(r_1+r_2)W}\right) + \left(A_{\text{H}}r_2^2 - A_{\text{S}}\right)\left(\mathrm{e}^{(r_1+r_2)W} - \mathrm{e}^{(r_2+r_3)W}\right) + \right.\\
&\left.\left(A_{\text{H}}r_3^2 - A_{\text{S}}\right)\left(\mathrm{e}^{(r_2+r_3)W} - \mathrm{e}^{(r_1+r_3)W}\right)\right](\psi_0 - \psi_1),
\end{aligned} \tag{8}$$

where $|A|$ is the coefficient determinate of Eq. (7), and L=$y_{\text{B}} - y_{\text{A}}$ denotes the length of the channel. Let

$$m_0 = -\frac{(y_B - y_A)}{\Delta f_0}\frac{r_1 r_2 r_3}{|A|}\left[\left(A_H r_1^2 - A_S\right)\left(e^{(r_1+r_3)W} - e^{(r_1+r_2)W}\right) + \left(A_H r_2^2 - A_S\right)\left(e^{(r_1+r_2)W} - e^{(r_2+r_3)W}\right) + \left(A_H r_3^2 - A_S\right)\left(e^{(r_2+r_3)W} - e^{(r_1+r_3)W}\right)\right], \quad (9)$$

we can then obtain the simultaneous equations for ψ_0 and ψ_1 as follows:

$$\psi_0 = \psi_{0,\text{ideal}} - m_0 T_1,$$
$$T_1 \equiv \psi_0 - \psi_1 = \frac{T_{1,\text{ideal}}}{1+\varepsilon_0 m_0}, \quad (10)$$

where $\varepsilon_0 = 1 + \frac{\Delta f_0}{\Delta f_1} - \frac{\Delta f_{ov1}}{\Delta f_1}$ and T_1 denotes the volume transported through the channel,

$$T_{1,\text{ideal}} \equiv \psi_{0,\text{ideal}} - \psi_{1,\text{ideal}} = \frac{1}{\Delta f_1}\oint_{C_1}\frac{\vec{\tau}}{\rho_0}\cdot d\vec{l} - \left(1 - \frac{\Delta f_{ov1}}{\Delta f_1}\right)\frac{1}{\Delta f_0}\oint_{C_0}\frac{\vec{\tau}}{\rho_0}\cdot d\vec{l}.$$

Similarly, when $\left(-\frac{\beta}{2A_H}\right)^2 - \left(\frac{A_S}{3A_H}\right)^3 > 0$, the corresponding homogeneous Eq. (6) has a solution in the form

$$\psi(x,y) = c_0 + c_1 e^{rx} + e^{ax}(c_2\cos(bx) + c_3\sin(bx)),$$

where r_1=r, r_2=a+bi, r_3=a–bi are the solutions of the characteristic equation. $c_0 = \frac{|D_1|}{|D|}$, $c_1 = \frac{|D_2|}{|D|}$, $c_2 = \frac{|D_3|}{|D|}$, $c_3 = \frac{|D_4|}{|D|}$, and $|D|$ is the coefficient determinant of the following equations:

$$\begin{aligned}
&c_0 + c_1 + c_2 = \psi_1,\\
&c_0 + c_1 e^{rW} + c_2 e^{aW}\cos(bW) + c_3 e^{aW}\sin(bW) = \psi_0,\\
&c_1 r + a c_2 + b c_3 = 0,\\
&c_1 r e^{rW} + (a e^{aW}\cos(bW) -\\
&e^{aW} b\sin(bW)) c_2 + (a e^{aW}\sin(bW) + e^{aW} b\cos(bW)) c_3 = 0;
\end{aligned}$$

$|D_i|$ is the determinant in which the i-th column is displaced by a constant term in the above coefficient determinant.

The dissipation along the integration path can also be calculated as

$$\begin{aligned}
F_0 &= \frac{1}{\Delta f_0}\int_A^B \vec{F}\cdot d\vec{l} \approx \frac{1}{\Delta f_0}\int_A^B \left[A_H\left(\frac{\partial^3\psi}{\partial x^3}\right)_{x=W} - A_S\left(\frac{\partial\psi}{\partial x}\right)_{x=W}\right] dy\\
&\approx \frac{(y_B - y_A)}{\Delta f_0}\left[A_H\left(\frac{\partial^3\psi}{\partial x^3}\right)_{x=W} - A_S\left(\frac{\partial\psi}{\partial x}\right)_{x=W}\right]\\
&= \frac{(y_B - y_A)}{\Delta f_0}[c_1 r e^{rW}(A_H r^2 - A_S) + c_2 e^{aW}[(a^3 A_H - 3ab^2 A_H - aA_S)\cos(bW) + (b^3 A_H - 3a^2 bA_H + bA_S)\sin(bW)] +\\
&\quad c_3 e^{aW}[(3a^2 bA_H - b^3 A_H - bA_S)\cos(bW) + (a^3 A_H - 3ab^2 A_H - aA_S)\sin(bW)]\\
&= \frac{(y_B - y_A)}{\Delta f_0 |D|}[(a^2+b^2)e^{aW}\sin(bW) r e^{rW}(A_H r^2 - A_S) + (br e^{rW} - rae^{aW}\sin(bW) - rbe^{aW}\cos(bW))e^{aW}\times\\
&\quad [(a^3 A_H - 3ab^2 A_H - aA_S)\cos(bW) + (b^3 A_H - 3a^2 bA_H + bA_S)\sin(bW)] +\\
&\quad (rae^{aW}\cos(bW) - rbe^{aW}\sin(bW) - are^{rW})e^{aW}[(3a^2 bA_H - b^3 A_H - bA_S)\times\\
&\quad \cos(bW) + (a^3 A_H - 3ab^2 A_H - aA_S)\sin(bW)]](\psi_0 - \psi_1).
\end{aligned} \quad (11)$$

Let

$$\begin{aligned}
r_0 = &-\frac{(y_B - y_A)}{\Delta f_0 |D|}[(a^2+b^2)e^{aW}\sin(bW) r e^{rW}(A_H r^2 - A_S) + (br e^{rW} - rae^{aW}\sin(bW) - rbe^{aW}\cos(bW))e^{aW}\times\\
&[(a^3 A_H - 3ab^2 A_H - aA_S)\cos(bW) + (b^3 A_H - 3a^2 bA_H + bA_S)\sin(bW)] + (rae^{aW}\cos(bW) - rbe^{aW}\sin(bW) - are^{rW})e^{aW}\times\\
&[(3a^2 bA_H - b^3 A_H - bA_S)\cos(bW) + (a^3 A_H - 3ab^2 A_H - aA_S)\sin(bW)]].
\end{aligned} \quad (12)$$

We have the corresponding simultaneous equations:

$$\psi_0 = \psi_{0,\text{ideal}} - r_0 T_1,$$
$$T_1 \equiv \psi_0 - \psi_1 = \frac{T_{1,\text{ideal}}}{1+\varepsilon_0 r_0}. \quad (13)$$

The transport is similar to that of Wajsowicz (2002), but r_0 and m_0 represent different frictional constants.

3 Effects of bottom and lateral dissipation

In Eqs (10) and (13), $\varepsilon_0 m_0$ and $\varepsilon_0 r_0$ reflect the effect of friction on the volume transport. For $\varepsilon_0 = 1 + \frac{\Delta f_0}{\Delta f_1} - \frac{\Delta f_{ov1}}{\Delta f_1}$, the relative size of the islands and the channel length affect the transport. The larger the western island, or the longer the channel between the islands, the more severe the shear velocity of the fluid in the channel, resulting in a larger volume transport. The combined dissipation factors m_0 and r_0 are the result of the combined action of the lateral friction and bottom friction. To examine the interaction between the two friction types and their influence on ψ, we limit our discussion to the barotropic beta plane. Combining the relationship between the roots and coefficients in the characteristic equation, the combined dissipation factors m_0 and r_0 have the following forms:

$$m_0 = \frac{L}{L_0}\frac{1}{|A|}\left[\left(r_1^2 - \frac{A_S}{A_H}\right)\left(e^{-r_2 W} - e^{-r_3 W}\right) + \left(r_2^2 - \frac{A_S}{A_H}\right)\times\left(e^{-r_3 W} - e^{-r_1 W}\right) + \left(r_3^2 - \frac{A_S}{A_H}\right)\left(e^{-r_1 W} - e^{-r_2 W}\right)\right] \quad (14)$$

and

$$r_0 = \frac{L}{L_0|D|}\left[e^{aW}\sin(bW)e^{rW}\left(r^2-\frac{A_S}{A_H}\right)+\left[\left(be^{rW}-ae^{aW}\sin(bW)-be^{aW}\cos(bW)\right)e^{aW}/(a^2+b^2)\right]\times\right.$$
$$\left[\left(a^3-3ab^2-a\frac{A_S}{A_H}\right)\cos(bW)+\left(b^3-3a^2b+b\frac{A_S}{A_H}\right)\sin(bW)\right]+\left[\left(ae^{aW}\cos(bW)-be^{aW}\sin(bW)-ae^{rW}\right)e^{aW}/(a^2+b^2)\right]\times$$
$$\left.\left[\left(3a^2b-b^3-b\frac{A_S}{A_H}\right)\cos(bW)+\left(a^3-3ab^2-a\frac{A_S}{A_H}\right)\sin(bW)\right]\right], \quad (15)$$

where L_0 denotes the length of the first island to the west of the landmass. Then, $\frac{L}{L_0}$ is the ratio between the lengths of the channel and the island. From Eqs (14) and (15) we see that m_0 and r_0 are both functions of A_H, A_S and W. The relationship is more complex from the analytic solution. For simplicity, we set $\frac{L}{L_0}$ and W as constants to derive the relationship among A_H, A_S, m_0 and r_0. Let $\frac{L}{L_0}$=0.6, W=100 km, A_S=x×10^{-6} m^2/s, A_H=y×10^4 m^2/s. For certain values of A_H and A_S, Fig. 3 shows the corresponding combined dissipation factors m_0 and r_0.

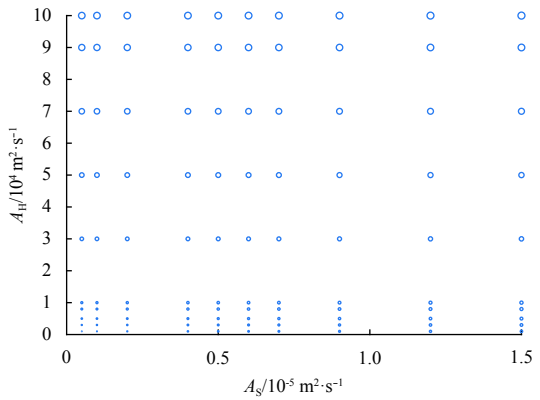

Fig. 3. Combined dissipation factor about A_H and A_S in the channel between the islands. The circles denote the combined dissipation factors and the size of the circles represent the magnitude of the combined dissipation factors. The single channel is shallow and narrow. The width of the channel is 100 km.

Figure 3 indicates that the combined dissipation factor is approximately a linear function of A_H when A_S is constant. Similarly, the combined dissipation factor is approximately a linear function of A_S when A_H is constant. Therefore, we can use linear regression to model the relationship between the two coefficients. Applying a partial F-test, under a 0.05 confidence level, we have

$$z = -0.314\,6+0.353\,5A_S+3.606\,4A_H, \quad (16)$$

where z denotes the estimated value of the combined dissipation factor m_0 or r_0. Thus, A_S and A_H have a linear influence on the combined dissipation factors m_0 and r_0. A_S has a greater impact on m_0 and r_0. The regression coefficient depends on the width of the channel. To study the effect of the channel width on the combined dissipation factor, we set A_H=10^4 m^2/s and D_f=2×10^{-3} m^2/s. When the depth changes, A_S changes and the expression $\left(\frac{-\beta}{2A_H}\right)^2-\left(\frac{A_S}{3A_H}\right)^3$ also changes. For convenience of reference, we set H_0=400 m and H_0=1 000 m. When H_0=400 m, then A_S=5×10^{-6} m^2/s and the combined dissipation factor is m_0. The m_0 values for different channel widths are shown in Fig. 4.

The coefficient m_0 decreases monotonically with increasing channel width (Fig. 4). Initially, m_0 decreases rapidly, then the rate slows with increasing width, and gradually m_0 approaches zero. This indicates an increase in the volume transport as the channel widens; initially the rate of increase is fast, then it slows, and finally stabilizes at the ideal value. Thus, the lateral friction and the bottom friction hinder the volume transport, having a relatively large effect at the beginning, which gradually weakens.

For H_0=1 000 m, A_S=2×10^{-6} m^2/s and the combined dissipation factor is r_0. The r_0 values for different channel widths are shown in Fig. 5.

The coefficient r_0 (Fig. 5) is positive and decreases with increasing width when the channel width is less than approximately 470 km. r_0 decreases rapidly initially, then at a slower rate, indicating that generally the friction hinders the volume transport; the narrower the channel, the stronger the effect. For channel widths between 470 km and 1 000 km, r_0 is negative, decreasing at first, and then increasing. The negative value indicates that the volume transport is larger than the ideal transport value and has a maximum level. In this case r_0 increases the volume transport, which is similar to the flow behavior when only lateral friction is considered. For channel widths over 1 000 km, although r_0 is positive, it is very small and the volume transport tends toward

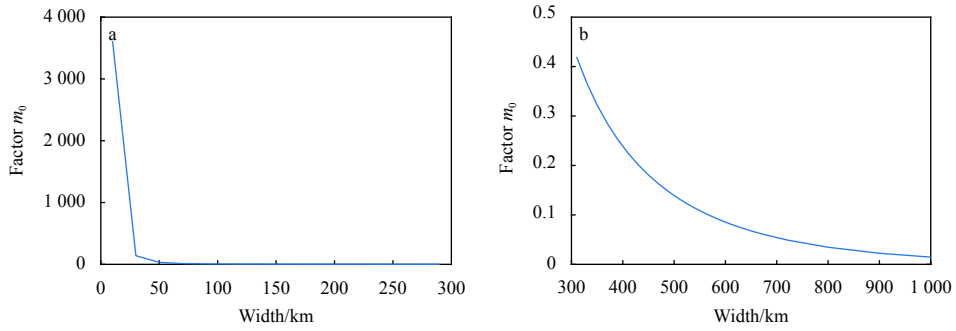

Fig. 4. The dissipation factor m_0 with increasing channel width between the two islands. The water depth is 400 m in a flat-bottom basin. Channel width is 0–300 km (a) and 300–1 000 km (b).

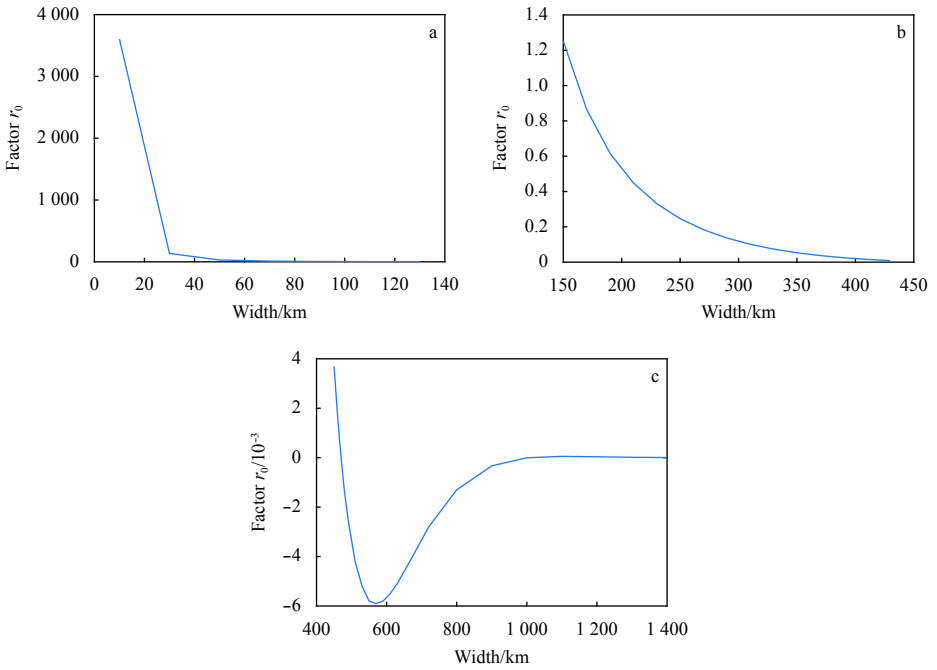

Fig. 5. The dissipation factor r_0 with increasing channel width between the two islands. The water depth is 1 000 m in a flat-bottom basin. Channel width is 0–140 km (a), 150–450 km (b) and 400–1 400 km (c).

the ideal value.

Comparing Figs 4 and 5, the effect of r_0 on the volume transport is more complicated than that of m_0. When the channel is narrow, m_0 is more effective in reducing the volume transport ratio than r_0. However, when the channel is wider, r_0 can increase the flow. Comparing the derivation process, the only difference lies in the depth. From $A_S = \frac{D_f}{H_0}$, A_S decreases when the depth H_0 increases. This dampens the effect of the bottom friction, reducing the volume transport ratio when A_H and D_f are constant.

4 Discussion on the dissipation factors

To further understand the role of the bottom and lateral friction dissipation in regulating the water flow, it is helpful to consider two islands of the same size lying in an enclosed barotropic ocean, as shown in Fig. 6. The width and length of the islands are 400 km×1 000 km, respectively, and the channel is W km wide and 600 km long. The depth of the ocean is constant at 400 m. We then have $\varepsilon_0 = 1 + \frac{\Delta f_0}{\Delta f_1} - \frac{\Delta f_{ov1}}{\Delta f_1} = \frac{7}{5}$. When the frictional dissipation in the channel is neglected, T_{ideal} can be obtained by Eqs (3) and (4) if the wind is given. Let A_H=10^4 m^2/s, A_S=5×10^{-6} m^2/s and β=2×10^{-11} m^{-1}·s^{-1}. The wind is $taux = taux_0 \times \cos\left(\frac{\pi \times y}{y_{max}}\right)$, where $taux_0$=0.1 N/m^2 and ρ=1.03×10^3 kg/m^3. Then the Munk frictional boundary layer thickness is $\delta_M = (A_H/\beta)^{\frac{1}{3}} \approx 80$ km.

Wajsowicz (1993) derived the streamfunctions considering either the bottom friction or the lateral. Here, we take both the bottom and lateral friction into account and calculate m_0 and the transport through the channel. To investigate the difference between the various transport formulas, the transport through the channel was calculated for various widths W using the different rules and models. The transport T is shown in Table 1 where T_{ideal} denotes the transport through the channel based on Godfrey's Island Rule (Eq. (12) in Godfrey (1989)). $T_{Stommel}$ denotes the transport through the channel based on Wajsowicz's Island Rule (Eq. (4.3) in Wajsowicz (1993)) which considers only the bottom friction. T_{Munk} denotes the transport through the channel by Wajsowicz's Island Rule (Eq. (4.5) in Wajsowicz (1993)) which considers only the lateral friction. $T_{together}$ denotes the transport

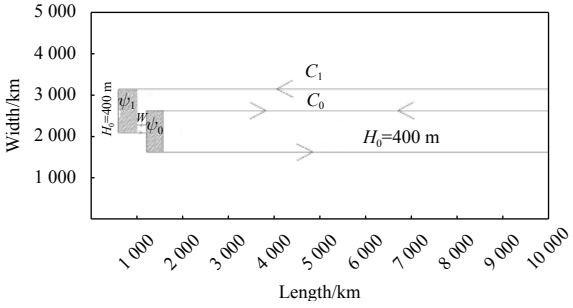

Fig. 6. The model basin and islands. For simplicity, the basin and the islands are rectangular. The islands are of the same size.

Table 1. The transport T through the channel for various channel widths using different transport models

	W							
	30 km	50 km	80 km	120 km	200 km	260 km	320 km	400 km
T_{ideal}/10^6 m^3·s^{-1}	0.978 0	1.038 0	1.128 0	1.249 0	1.489 0	1.670 0	1.850 0	2.091 0
$T_{Stommel}$/10^6 m^3·s^{-1}	0.122 3	0.2	0.311 2	0.454 2	0.726 3	0.923 8	1.117	1.371 1
T_{Munk}/10^6 m^3·s^{-1}	0.007 3	0.035	0.140 5	0.405 1	1.026 9	1.386 1	1.666 8	1.979 6
$T_{together}$/10^6 m^3·s^{-1}	0.005 0	0.023	0.083 2	0.223 6	0.604 0	0.906 7	1.200 5	1.572 9

through the channel by considering both the lateral and bottom friction (Eq. (10) or Eq. (13)).

Figure 7a shows the transport through the channel for various channel widths calculated by three different methods: T_{ideal}, T_{Munk} and $T_{together}$. In all three cases, the transport increases with the increasing widths. Compared with $T_{together}$, T_{Munk} lacks the bottom friction, and the rate of increase is different with increasing width. In general, $T_{together}<T_{Munk}$; as Wajsowicz (1993) noted, the bottom friction reduces the volume transport but cannot reverse the flow direction between the two islands. As $W<\delta_M$, $T_{together}<<T_{ideal}$, and $T_{Munk}<<T_{ideal}$, indicating that the lateral friction and bottom friction greatly reduce the transport. The role of the lateral friction is greater than that of the bottom friction in the Munk boundary layer thickness; therefore $T_{together} \cong T_{Munk}$. Beyond the Munk boundary layer thickness, T_{Munk} increases rapidly, then more slowly but almost always at a higher rate than $T_{together}$, because the role of the lateral friction weakens. When $W>250$ km, we have $T_{together}<T_{Munk}$ and $T_{ideal}-T_{Munk}<<T_{ideal}-T_{together}$ because the role of the bottom friction is greater than that of the lateral friction. At this point, if only the lateral friction is considered to estimate the volume transport through the channel, the results would be unreasonable.

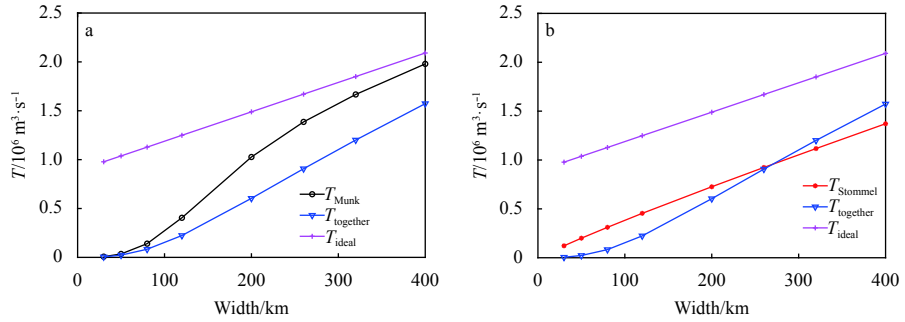

Fig. 7. Transport values through the channel for various channel widths calculated by four methods. The blue line denotes $T_{together}$, the black line T_{Munk}, the red line $T_{Stommel}$ and the pink line T_{ideal}.

Similarly, Fig. 7b shows the transport through the channel for various channel widths calculated by T_{ideal}, $T_{Stommel}$ and $T_{together}$. $T_{together}$ has more lateral friction than $T_{Stommel}$. Although $T_{Stommel}$ and $T_{together}$ increase with increasing channel width, the slopes of the curves are different. As in the case of T_{Munk}, $T_{Stommel}$ is much larger than $T_{together}$ within the Munk layer because of the role of the lateral friction. Beyond the Munk layer, the difference between $T_{Stommel}$ and $T_{together}$ becomes smaller as the channel widens. This shows that the combined effect of the lateral friction and bottom friction is to reduce the transport, the bottom friction being the dominant force. When $W\approx270$ km, we have $T_{Stommel}=T_{together}$; thus, the lateral friction has little effect on the volume transport through the channel. At a certain range, however, when $W>270$ km, $T_{together}>T_{Stommel}$, indicating that the lateral friction is enhancing the flow, as Pratt and Pedlosky (1998) verified after examining the velocity structure of the lateral boundary layer solution. When the island is placed to prevent the reverse flow but not the direct flow, the transport through the channel is larger than what is transported by the lateral boundary layer as a whole. This suggests that the lateral friction affects the transport.

5 Application to the Indonesian throughflow

In our study, the volume transport through the channel between the islands is obtained by considering the Munk-Stommel model. The results are similar to those of Wajsowicz (1993, 2002), but the frictional constants are different. Equations (14) and (15) indicate that the frictional constants m_0 and r_0 depend on the width W, the horizontal eddy viscosity A_H and the bottom drag coefficient D_f. In the case of real ocean islands, only broad estimates of these values are known. Here, as a case study we calculate the Indonesian throughflow transport (ITFT). Using the frictionless Island Rule (Godfrey, 1989) the ITF yielded a mean annual ITFT estimate of approximately 13.865 0×10^6 m^3/s by integrating wind-stress data from 1958 to 2001 (Liu et al., 2007). The bulk of the ITF is thought to cross the Makassar Strait, with smaller volumes transported through the other straits (Masumoto and Yamagata, 1996; Metzger and Hurlburt, 1996). Although the ITF is not barotropic, the bulk of the volume transport is considered to be confined to the upper 200–300 m. A barotropic model where all the bottom topography is assumed constant may serve as an approximation to the throughflow. The frictional channel runs from the equator to 12°S. Hence, assuming Australia-PNG extends 45°S. Thus, the upper limit ratio on $\frac{L}{L_0}$ is 0.3 (Pratt and Pedlosky, 1998). Let H_0=300 m, using the published coefficient estimates $A_H=10^4$ m^2/s, $D_f=2\times10^{-3}$ m^2/s, we obtain $A_S=2/3\times10^{-5}$ m^2/s. Taking the width W=300 km (Wajsowicz, 1993; Lian et al., 2017), we can derive the frictional constant m_0=–0.312 8 and an annual mean ITFT estimate of approximately 10.561 4×10^6 m^3/s using Eqs (13) and (14). Thus, the transport decreases by 3.303 6×10^6 m^3/s, accounting for 23.8% of the annual mean ITFT of 13.865 0×10^6 m^3/s. If $A_H=5\times10^3$ m^2/s, $D_f=5\times10^{-4}$ m^2/s and H_0=200 m, as estimated based on Wajsowicz (1993) and Pratt and Pedlosky (1998), we can derive the frictional constant m_0=–0.199 1 and an estimated annual mean ITFT of approximately 11.562 8×10^6 m^3/s, accounting for 16.6% of the annual mean ITFT. The Island Rule is generally found to overestimate the volume transport by 0%–25%, primarily because it neglects the friction (Pedlosky, 1996). The result is consistent with Pedlosky's findings.

6 Summary

In this paper an explicit Island Rule which considers both lateral and bottom friction is presented. It is valid when the width of the channel is much smaller than its length in a flat-bottom ocean. The estimate of the flow reduction applies when the island is located within the western boundary layer, where the friction is significant along the coast of the island. For the dissipation factor that combines the lateral and bottom friction, an ap-

proximately linear relationship was found between the lateral and bottom friction for a constant width by using randomly chosen values. In discussing the influence of the channel width on the combined dissipation factor when the lateral coefficient and the bottom drag coefficient are constant, $\left(\frac{-\beta}{2A_{\mathrm{H}}}\right)^2-\left(\frac{A_{\mathrm{S}}}{3A_{\mathrm{H}}}\right)^3$ =0 is the demarcation point; hence, the depth is a dominant factor. The combined dissipation factor reduces the flow in shallow water but can enhance the flow for some widths in deep water. We compared our model of two islands with the model of Wajsowicz with different channel widths. The results showed that the lateral coefficient is important when the channel narrow, and the bottom coefficient is important when the width is wide.

The validity of these conclusions is limited by the conditions that the width of the channel is much smaller than its length in a flat-bottom ocean. In the real ocean, some channels do not meet these conditions. Wajsowicz (1993), Lian et al. (2017) and Yang et al. (2013) investigated the bottom pressure torque or topographic effect on the Island Rule. When the width of the channel is not much smaller than the length, Eq. (5) does not apply and the wind in the channel causes a Sverdrup flow which cannot be ignored. Future work should examine methods to derive the combined dissipation factor from Eq. (6).

References

Cai W. 2006. Antarctic ozone depletion causes an intensification of the Southern Ocean super-gyre circulation. Geophysical Research Letters, 33(3): L03712

Chen Zhaohui, Wu Lixin, Qiu Bo, et al. 2014. Seasonal variation of the south equatorial current bifurcation off Madagascar. Journal of Physical Oceanography, 44(2): 618–631, doi: 10.1175/JPO-D-13-0147.1

Firing E, Qiu Bo, Miao Weifeng. 1999. Time-dependent Island Rule and its application to the time-varying north Hawaiian ridge current. Journal of Physical Oceanography, 29(10): 2671–2688, doi: 10.1175/1520-0485(1999)029<2671:TDIRAI>2.0.CO;2

Godfrey J S. 1989. A Sverdrup model of the depth-integrated flow for the world ocean allowing for island circulation. Geophysical and Astrophysical Fluid Dynamics, 45(1): 89–112

Godfrey J S. 1996. The effect of the Indonesian Throughflow on ocean circulation and heat exchange with the atmosphere: A review. Journal of Geophysical Research: Oceans, 101(C5): 12217–12237, doi: 10.1029/95JC03860

Gordon L A, Sprintall J, Van Aken H M, et al. 2010. The Indonesian Throughflow during 2004-2006 as observed by the instant program. Dynamics of Atmospheres and Oceans, 50(2): 115–128, doi: 10.1016/j.dynatmoce.2009.12.002

Gordon L A, Susanto L, Field R D. 1999. Throughflow within Makassar strait. Geophysical Research Letter, 26(21): 3325–3328, doi: 10.1029/1999GL002340

Gordon L A, Susanto D R, Vranes K. 2003. Cool Indonesian Throughflow as a consequence of restricted surface layer flow. Nature, 425(6960): 824–828, doi: 10.1038/nature02038

Lian Zhan, Fang Guohong, Wang Xinyi, et al. 2017. Application of Multi-Island rule to the study of the inter-ocean circulation of the South China Sea. Advances in Marine Science (in Chinese), 35(1): 20–31

Liu Qinyan, Wang Dongxiao, Xie Qiang. 2012. The South China Sea Throughflow: linkage with local monsoon system and impact on upper thermal structure of the ocean. Chinese Journal of Oceanology and Limnology, 30(6): 1001–1009, doi: 10.1007/s00343-012-1303-8

Liu Qinyan, Wang Dongxiao, Xie Qiang, et al. 2007. Decadal variability of Indonesian Throughflow and South China Sea Throughflow and its mechanism. Journal of Tropical Oceanography (in Chinese), 26(6): 1–6

Liu Qinyan, Wang Dongxiao, Zhou Wen, et al. 2010. Covariation of the Indonesian Throughflow and South China Sea Throughflow associated with the 1976/77 regime shift. Advances in Atmospheric Sciences, 27(1): 87–94, doi: 10.1007/s00376-009-8061-3

Masumoto Y, Yamagata T. 1996. Seasonal variations of the Indonesian Throughflow in a general ocean circulation model. Journal of Geophysical Research: Atmospheres, 101(C5): 12287–12293, doi: 10.1029/95JC03870

Metzger E J, Hurlburt H E. 1996. Coupled dynamics of the South China Sea, the Sulu Sea, and the Pacific Ocean. Journal of Geophysical Research: Atmospheres, 101(C5): 12331–12352, doi: 10.1029/95JC03861

Pedlosky J. 1996. Ocean Circulation Theory. New York: Springer, 1–198

Pedlosky J, Pratt L, Spall M A, et al. 1997. Circulation around islands and ridges. Journal of Marine Research, 55(6): 1199–1251, doi: 10.1357/0022240973224085

Pedlosky J, Spall M. 1997. Rossby normal modes in basins with barriers. Journal of Physical Oceanography, 29(9): 2332–2349

Pratt L, Pedlosky J. 1998. Barotropic circulation around islands with friction. Journal of Physical Oceanography, 28(11): 2148–2162, doi: 10.1175/1520-0485(1998)028<2148:BCAIWF>2.0.CO;2

Qu Tangdong. 2000. Upper-layer circulation in the South China Sea. Journal of Physical Oceanography, 30(6): 1450–1460, doi: 10.1175/1520-0485(2000)030<1450:ULCITS>2.0.CO;2

Qu Tangdong, Du Yan, Sasaki H. 2006. South China Sea Throughflow: A heat and freshwater conveyor. Geophysical Research Letters, 33(23): L23617, doi: 10.1029/2006GL028350

Qu Tangdong, Kim Y Y, Yaremchuk M, et al. 2004. Can Luzon Strait transport play a role in conveying the impact of ENSO to the South China Sea?. Journal of Climate, 17(18): 3644–3657, doi: 10.1175/1520-0442(2004)017<3644:CLSTPA>2.0.CO;2

Seung Y H. 2003. Significance of shallow bottom friction in the dynamics of the Tsushima Current. Journal of Oceanography, 59(1): 113–118, doi: 10.1023/A:1022828825667

Wajsowicz R C. 1993. The circulation of the depth-integrated flow around an island with application to the Indonesian Throughflow. Journal of Physical Oceanography, 23(7): 1470–1484, doi: 10.1175/1520-0485(1993)023<1470:TCOTDI>2.0.CO;2

Wajsowicz R C. 1994. A relationship between interannual variations in the South Pacific wind stress curl, the Indonesian Throughflow, and the West Pacific warm water pool. Journal of Physical Oceanography, 24(10): 2180–2187, doi: 10.1175/1520-0485(1994)024<2180:ARBIVI>2.0.CO;2

Wajsowicz R C. 2002. A modified Sverdrup model of the Atlantic and Caribbean circulation. Journal of Physical Oceanography, 32(3): 973–993, doi: 10.1175/1520-0485(2002)032<0973:AMSMOT>2.0.CO;2

Wajsowicz R C. 2010. The response of the Indo-Pacific Throughflow to interannual variations in the Pacific wind stress. Part I: idealized geometry and variations. Journal of Physical Oceanography, 25(8): 1805–1826

Wang Dongxiao, Liu Qinyan, Huang Ruixin, et al. 2006. Interannual variability of the South China Sea Throughflow inferred from wind data and an ocean data assimilation product. Geophysical Research Letters, 33(14): L14605, doi: 10.1029/2006GL026316

Wijffels S E, Bray N, Hautala S, et al. 1996. The WOCE Indonesian Throughflow repeat hydrography sections: I10 and IR6. International WOCE Newsletter, 24: 25–28

Yang Jiayan, Lin Xiaopei, Wu Dexing. 2013. On the dynamics of the seasonal variation in the South China Sea Throughflow transport. Journal of Geophysical Research: Oceans, 118(12): 6854–6866, doi: 10.1002/2013JC009367